Atmos. Chem. Phys. Discuss., 10, 3087–3127, 2010
www.atmos-chem-phys-discuss.net/10/3087/2010/

Atmospheric Chemistry and Physics Discussions

This discussion paper is/has been under review for the journal Atmospheric Chemistry and Physics (ACP). Please refer to the corresponding final paper in ACP if available.

Quantification of DMS aerosol-cloud-climate interactions using ECHAM5-HAMMOZ model in current climate scenario

M. A. Thomas[1], P. Suntharalingam[1], L. Pozzoli[2], S. Rast[3], A. Devasthale[4], S. Kloster[5,3], J. Feichter[3], and T. M. Lenton[1]

[1]School of Environmental Sciences, University of East Anglia, Norwich, UK
[2]Climate Change Unit, Joint Research Center, Italy
[3]Max-Planck-Institute for Meteorology, Hamburg, Germany
[4]Swedish Meteorological and Hydrological Institute, Norrkoping, Sweden
[5]Earth and Atmospheric Sciences, Cornell University, Ithaca, NY, USA

Received: 11 December 2009 – Accepted: 27 January 2010 – Published: 5 February 2010

Correspondence to: M. A. Thomas (manu.thomas@uea.ac.uk)

Published by Copernicus Publications on behalf of the European Geosciences Union.

Abstract

The contribution of ocean dimethyl sulfide (DMS) emissions to changes in cloud microphysical properties is quantified seasonally and globally for present day climate conditions using an aerosol-chemistry-climate general circulation model, ECHAM5-HAMMOZ, coupled to a cloud microphysics scheme. We evaluate DMS aerosol-cloud-climate linkages over the southern oceans where anthropogenic influence is minimal. The changes in the number of activated particles, cloud droplet number concentration (CDNC), cloud droplet effective radius, cloud cover and the radiative forcing are examined by analyzing two simulations: a baseline simulation with ocean DMS emissions derived from a prescribed climatology and one in which the ocean DMS emissions are switched off. Our simulations show that the model realistically simulates the seasonality in the number of activated particles and CDNC, peaking during Southern Hemisphere (SH) summer coincident with increased phytoplankton blooms and gradually declining with a minimum in SH winter. In comparison to a simulation with no DMS, the CDNC level over the southern oceans is 128% larger in the baseline simulation averaged over the austral summer months. Our results also show an increased number of smaller sized cloud droplets during this period. We estimate a maximum decrease of up to 15–18% in the droplet radius and a mean increase in cloud cover by around 2.5% over the southern oceans during SH summer in the simulation with ocean DMS compared to when the DMS emissions are switched off. The global annual mean top of the atmosphere DMS aerosol all sky radiative forcing is $-2.03\,W/m^2$, whereas, over the southern oceans during SH summer, the mean DMS aerosol radiative forcing reaches $-9.32\,W/m^2$.

1 Introduction

Research on phytoplankton induced dimethyl sulfide (DMS) emissions from the global oceans and their potential impact on the climate was stimulated by the publication of

ACPD

10, 3087–3127, 2010

the CLAW hypothesis in 1987 (Charlson et al., 1987). This hypothesis suggested the linkages between the following processes:

1. In a warmer world enhanced phytoplankton blooms would result in increased ocean DMS concentrations and an increased flux of DMS to the atmosphere.

2. DMS is oxidized in the atmosphere and forms SO_4 which nucleates or condenses on existing particles to form sulfate aerosols.

3. These aerosols have the capability to act as cloud condensation nuclei (CCN) and an increase or decrease in their concentrations could modulate the planetary albedo thereby affecting the climate.

However, the exact contribution of the individual processes in this proposed feedback loop remains poorly characterized and therefore, our focus here is to separately quantify elements of the connecting links in this loop in a present day climate scenario.

A range of observational studies have explored the potential links between ocean DMS emissions and climate. Field studies investigating the links between DMS emissions and CCN yield mixed conclusions (Hegg et al., 1991; Andreae et al., 1995; O'Dowd et al., 1997). One reason could be that the time scale of aerosol and CCN formation from DMS oxidation (several days to weeks) complicates the interpretation of the field measurements (Korhonen et al., 2008). A clearer relationship of the DMS-CCN link has been established from two marine measurement stations with long term CCN records, and from satellite sensors. Observations at Cape Grim, Tasmania (41° S) show similar seasonal cycles for atmospheric DMS and CCN concentrations; the CCN concentrations were 2–3 times higher in summer than in winter coinciding with the phytoplankton blooms in the summer (Ayers and Gras, 1991). Short-term airborne measurements close to the site indicate that CCN concentrations can be more than an order of magnitude higher in summer than in JJA (Yum and Hudson, 2004). These local observations are consistent with seasonal changes in cloud optical depth observed by satellite near Cape Grim (Boers et al., 1994). Measurements at the Mace Head

ACPD
10, 3087–3127, 2010

Irish coastal site (53.19° N, 9.54° W) indicated the highest CCN concentrations during the biologically productive season when the DMS emissions are expected to be high (Reade et al., 2006). This site, however, does not have continuous measurements of atmospheric DMS concentration, hence the DMS-CCN link could not be more clearly demonstrated over the seasonal cycle. Similar studies carried out over the Pacific ocean (1982–1985) also revealed that the area weighted concentrations were higher in summer than in winter (Bates et al., 1987) and that the changes in atmospheric and oceanic properties associated with El Nino events do not significantly affect the DMS sea water concentrations over the equatorial Pacific ocean (15° N–15° S) (Bates and Quinn, 1997). Studies using remote sensing data have also investigated the relationships between oceanic DMS and CCN. Vallina and Simo (2007) showed that DMS emissions can contribute to up to 30% of the globally averaged annual CCN column concentration, but, can be highly variable spatially. Meskhidze and Nenes (2006) using satellite data reported a good correlation between the chlorophyll-A from SeaWIFS (Sea-viewing Wide Field-of-view Sensor) and CCN (positively correlated) and cloud droplet effective radii (negatively correlated) derived from MODIS (Moderate Resolution Imaging Spectroradiometer) over the 49° S–54° S latitude band. There is still uncertainty in the dependence of DMS flux on the chlorophyll-A concentration as only certain species of phytoplankton produce DMS. The study by Leck et al. (1990) revealed that the DMS concentration may be related to the phytoplankton growth under nitrogen limited conditions.

Modeling studies have also investigated the response of oceanic DMS sea surface concentration to changes in climate. Kloster et al. (2007) applied the ECHAM5 atmospheric model coupled to an ocean model and a marine biogeochemistry model in a transient climate simulation, and analyzed the changes in DMS sea surface concentrations induced by changes in climate. However, their study did not evaluate the DMS derived changes in the cloud microphysical properties. Gunson et al. (2006) evaluated the DMS-CCN-temperature link by using the Hadley Center coupled ocean atmosphere model, HADCM3. Their study quantified changes to cloud cover and cloud albedo

for varying ocean DMS emissions, and reported global surface temperature changes of −0.8 °K and +1.5° K for scenarios where DMS flux to the atmosphere is doubled and halved respectively. Korhonen et al. (2008) used an offline global atmospheric chemistry transport model with size resolved aerosol microphysics (GLOMAP-bin) to investigate the influence on CCN over the Southern Hemisphere ocean. They found a moderate contribution of DMS to regional CCN, smaller than that suggested by previous satellite data analysis. Their study also suggested that the main pathway of DMS influence on CCN number is nucleation of DMS derived H_2SO_4 in the free troposphere and subsequent growth by condensation and coagulation. A perturbed DMS patch in the southern oceans induces high CCN concentrations several thousand kilometers downwind of the patch due to the time scale (several days) of conversion from DMS into CCN (Woodhouse et al., 2008). Gondwe et al. (2003), using a global three dimensional chemistry transport model estimated the contribution of sea water DMS to the mean annual column burden of $nssSO_4^=$ (non sea salt sulfate) in the SH as 43%, in comparison to the NH where it is only 9%. Kloster et al. (2006) also obtained similar estimates with DMS derived $nssSO_4^=$ contributions of 45% in the SH and 18% in the NH.

The majority of these modeling studies report DMS derived influences as global mean values. They do not focus on the spatial and temporal variations of the cloud microphysical properties and climate or were unable to assess these changes in their model. In this study we use the state of the art aerosol-chemistry-climate general circulation model (GCM), ECHAM5-HAMMOZ to quantify the influence of oceanic DMS emissions on the individual processes and variables in the DMS-aerosol-cloud-climate loop proposed by CLAW. This study represents the first such model analysis to investigate the impact on cloud microphysics and climate using a GCM with coupled aerosol-chemistry. We evaluate the spatial and temporal distributions of the conversion of the ocean DMS to atmospheric H_2SO_4 concentrations in liquid phase. We also assess changes in the cloud microphysical properties, for example, changes in the cloud droplet concentration, cloud droplet radius and cloud cover, induced by changes

in ocean DMS.

We focus, in particular, over the southern oceans during the SH summer months when DMS sea water concentrations are high (Kettle and Andreae, 2000; Kettle et al., 1999). Moreover, this remote marine lower troposphere is an ideal region for studying DMS-aerosol-cloud-climate interactions as it is a region of abundant low level clouds and is relatively unaffected by anthropogenic emissions.

2 ECHAM5-HAMMOZ model, experimental set up and simulations

The ECHAM5-HAMMOZ model used in the present study has three main components: the general circulation model, ECHAM5 (Roeckner and co authors, 2003), the tropospheric chemistry module, MOZ that is based on the chemical mechanism described by Horowitz et al. (2003) and the aerosol module, HAM (Hamburg Aerosol Model) (Stier et al., 2005). The ECHAM5 model is coupled to a detailed cloud microphysics module (Lohmann et al., 1999, 2007). A description of the respective modules is given in Pozzoli et al. (2008a). The chemistry and aerosol modules interact through three main mechanisms namely, photolytic reactions, sulfur chemistry and heterogeneous chemistry. The HAM module takes into account the major aerosol compounds: sulfate, black carbon, organic carbon, sea salt and mineral dust. The aerosol spectrum is represented by the combination of seven lognormal modes and these modes are described by the aerosol number, the number median radius and the standard deviation. Aerosols are categorized by size into nucleation, Aitken, accumulation and coarse modes. Mineral dust and sea salt emissions are calculated interactively following the parameterization schemes of Tegen et al. (2002) and Schulz et al. (2004), respectively. The MOZ chemical scheme is identical to the one used in the MOZART-2 model and includes 63 tracers and 168 reactions to represent O_x-NO_x-hydrocarbon chemistry.

The pathway from DMS emissions to the cloud droplet formation in the model is shown schematically in Fig. 1. The DMS sea water concentrations are prescribed in the model from the climatology of Kettle and Andreae (2000). The DMS flux to the

ACPD
10, 3087–3127, 2010

atmosphere is based on the parameterization of Nightingale et al. (2000). The MOZ component of the model considers two major reaction pathways for the conversion of atmospheric DMS to SO_2: (1) an abstraction pathway following a daytime reaction with OH and a nighttime reaction with NO_3 and (2) an addition pathway that leads to the formation of 75% SO_2 and 25% Methyl sulfonic acid (MSA) (Feichter et al., 1996). The SO_2 is oxidized to H_2SO_4, whereas MSA is directly converted to H_2SO_4 in the gas phase. The H_2SO_4 in the gas phase is passed into the HAM module for the subsequent conversion to sulfate aerosol. The main processes considered here are: (1) nucleation of new particles and subsequent growth by coagulation and condensation and (2) condensation on all aerosol modes (Stier et al., 2005). The cloud scheme in the model is based on the modified version by Lohmann and Roeckner (1996). The number of cloud droplets is parameterized as a function of the total aerosol number concentrations, updraft velocity and a shape parameter that takes into account the aerosol composition and the size distribution. In-cloud oxidation of SO_2 and resulting sulfate formation is also considered using the calculated oxidant fields of O_3 and H_2O_2.The heterogeneous reaction of SO_2 on sea salt aerosols and mineral dust particles is included in the sulfur chemistry of the ECHAM5-HAMMOZ model.

Simulations are performed with a spectral resolution of T42 that corresponds to approximately 2.8×2.8 degrees horizontally, with 31 vertical levels from the surface up to 10 hPa and with a 20-min time step. The model is driven by ECMWF ERA-40 meteorological fields (available every 6 h) (Uppala et al., 2005). In this configuration, the prognostic variables of ECHAM5 (vorticity, divergence, temperature and surface pressure) are relaxed towards the ERA-40 reanalysis data (Machenhauer and Kirchner, 2000). To evaluate the influence of DMS emissions on aerosol formation, cloud properties and climate variables, we carry out two 1-year simulations from Dec 1999 to Dec 2000: (1) the baseline simulation with prescribed DMS sea water concentrations (CTRL); and (2) a simulation with no ocean DMS (wo_ODMS). Other emissions (anthropogenic and wildfire) of SO_2, black carbon and organic carbon form the background aerosol concentrations, and are held fixed in our simulations in addition to the interac-

tively computed sea salt and dust emissions. An 18-month spin up is conducted for these simulations. We analyze the differences between these two simulations (CTRL – wo_ODMS) to identify the influence of ocean DMS on tropospheric aerosols, cloud properties and climate, focussing in particular on the southern ocean latitudes.

2.1 Model performance

Model evaluation of individual components of ECHAM5-HAMMOZ modules has been presented in several recent studies. The ECHAM5-HAM model has been comprehensively evaluated by Stier et al. (2005) who found good agreement between simulated and observed sulfate, black carbon and organic carbon surface concentrations regionally. The simulation of global annual mean aerosol optical depth agrees well with the MODIS satellite retrievals and with the AERONET[1] measurements. Additionally, the cloud microphysics scheme in the ECHAM5-HAM model was validated by Lohmann et al. (1999, 2007) who found that the simulated mean liquid water path, column CDNC and effective radius agree well with satellite observations and the frequency distributions of column CDNC over oceans and the variations of cloud optical depth with effective radius are simulated realistically.

The ECHAM5-MOZ model was also assessed against observations by Rast et al. (2010), Pozzoli (2007) and Auvray et al. (2007), who noted that several characteristics of the tropospheric spatial and temporal distribution, such as seasonal cycles and latitudinal gradients, are captured by the model. The comparison of the ECHAM5-HAMMOZ model with TRACE-P[2] aircraft campaign measurements showed that sulfate aerosol concentrations are generally well described in the north Pacific, but overestimated by a factor of 2 between 10° N and 25° N. This is a region of high aerosol loading, where sulfate concentrations depend mainly on the continental outflow of SO_2 and sulfate. The region under investigation in our study is a remote region in the high latitude

[1] AERONET: AErosol RObotic NETwork

[2] TRACE-P: TRAnsport and Chemical Evolution over the Pacific

ACPD
10, 3087–3127, 2010

SH, where the sulfate concentrations are mainly dependent on DMS oxidation. The Northern Hemisphere sulfate concentration does not influence the values in our study region.

In general, a good agreement was found between modeled aerosol optical depth in Southern Hemisphere compared with satellite observations (Stier et al., 2005; Pozzoli et al., 2008b). The size distribution, number concentration and optical properties are reproduced well by the coupled model, though the agreement is better near the surface than in the upper troposphere, where the model underestimates these parameters. Pozzoli et al. (2008b) found that annual mean burdens for the aerosol species using ECHAM5-HAMMOZ model did not differ significantly from those found with ECHAM5-HAM by Stier et al. (2005). ECHAM5-HAMMOZ showed some regional improvements for sulfate, especially in comparison to the EMEP[3] and IMPROVE[4] observations over Europe and US, respectively. The improvements are very likely due to an improved representation of the OH concentrations in ECHAM5-HAMMOZ which calculates OH concentrations interactively, in comparison to the climatological values used in ECHAM5-HAM (Sect. 4 in the supplementary online material of Pozzoli et al., 2008b).

2.2 Comparison of ECHAM5-HAMMOZ baseline configuration with previous studies/satellite observations

The DMS aerosol-cloud-climate simulation analyzed in this study has not been previously published. We therefore discuss the characteristics of this simulation here and compare to in-situ and satellite observations. Model variables evaluated include the simulated DMS flux to the atmosphere (Fig. 2), the tropospheric sulfate distribution (Fig. 3) and cloud properties namely, droplet radius and number concentrations and cloud liquid water path (Table 1). These are discussed in more detail below.

[3]EMEP: European Monitoring and Evaluation Programme

[4]IMPROVE: Interagency Monitoring of PROtected Visual Environments

We first consider the simulated global annual mean DMS flux to the atmosphere. The model estimates a global annual DMS flux of 23.3 Tg(S)/yr based on the gas exchange parameterization of Nightingale et al. (2000) and the Kettle and Andreae (2000) ocean DMS climatology. Other DMS flux estimates reported differ depending on the choice of the DMS sea surface climatology, gas exchange scheme and wind speed data; estimates vary from 16 Tg(S)/yr to 54 Tg(S)/yr (Kettle and Andreae, 2000). Our simulated global annual mean DMS flux is in close agreement with the findings of Boucher et al. (2003) who derived a global flux of 24–27 Tg(S)/yr based on the winds from the LMD-ZT general circulation model and the Nightingale et al. (2000) gas exchange.

Next, we compare the model generated seasonal cycle and magnitude of the ocean DMS flux to the atmosphere. Figure 2 presents the seasonal (three month averages) and spatial distribution of the DMS flux to the atmosphere in the baseline CTRL configuration (units of Kg(S)/m^2/s). We focus on the southern high latitudes from 30° S to 75° S. The seasonal cycle of the DMS emissions is distinct peaking in SH summer months (Dec-Jan-Feb (DJF) 1999/2000) coinciding with the peak in ocean biological activity and gradually declining with a minimum averaged over June, July and August (JJA) (Boers et al., 1996, 1998; Ayers and Gillett, 2000). This seasonality is consistent with the temporal variation in chlorophyll concentrations derived from SeaWIFS (Meskhidze and Nenes, 2006) satellite data. Peak DMS fluxes exceed 10×10^{-12} Kg(S)/m^2/s in localized high latitude regions during austral summer months (DJF 1999/2000) with a mean value of 4×10^{-12} Kg(S)/m^2/s in the latitudinal belt of 30° S–75° S. The mean winter fluxes are around 0.7×10^{-12} Kg(S)/m^2/s, almost one-eighth the mean summer fluxes in the southern belt (30° S–75° S).

The global seasonal distribution of the mass mixing ratios of atmospheric H_2SO_4 at 850 hPa is shown in Fig. 3. Concentrations ranging from 1.5×10^{-12} to as high as 3.0×10^{-12} are simulated at 850 hPa over the southern most latitude belt (60° S–75° S) during the SH summer months. The model produces a DJF mean concentration of 0.75×10^{-12} whereas the JJA mean is 0.11×10^{-12} at 850 hPa over the 30° S–75° S latitude belt. The seasonal variation in modelled $nssSO_4^=$ in our CTRL simulation is

ACPD
10, 3087–3127, 2010

comparable to those of Gondwe et al. (2003) who used a 3D global chemistry transport model, TM3, to evaluate the contribution of ocean DMS emission to the column burden of $nssSO_4^=$. Their study find a 6–8 times increase in the DJF mean $nssSO_4^=$ compared to the JJA mean over the southern belt (30° S–75° S) which is comparable to our value of ∼7.

The H_2SO_4 concentrations at 700 hPa also follow the spatial distribution at 850 hPa (Fig. A1). The concentrations at 700 hPa in the March-April-May (MAM) seasonal mean is about half of the DJF seasonal mean. However, the H_2SO_4 concentrations during the SH autumnal months are higher at 700 hPa than at 850 hPa.

Satellite sensors provide valuable information on cloud properties. Since the focus of this study is on aerosol-cloud interactions over the southern oceans during austral summer, we compare three important model parameters in this context, namely, CDNC, cloud droplet (CD) effective radii and cloud liquid water path with satellite data. We use effective radii and cloud optical depth information from PATMOS-x (AVHRR Pathfinder Atmospheres – Extended) to calculate adiabatic CDNC (Quaas et al., 2006). Additionally, we use cloud liquid water path from the most recent HOAPS (Hamburg Ocean Atmosphere Parameters and fluxes from Satellite data) (Andersson et al., 2007) Version-3 data set. These two data sets are available for the DJF 1999/2000 over the southern oceans in the latitudinal belt of 30° S–60° S, enabling comparison for the same time period with our model simulations.

Table 1 shows the comparison of satellite data with model estimates. The CD effective radii agree closely with satellite data over the southern oceans during austral summer, where the baseline model simulation estimates a mean droplet radius of 11.39 µm, compared to the mean satellite estimate of 11.61 µm. This is also consistent with the comparison reported by Lohmann et al. (1999) for ECHAM5. The agreement between simulated and satellite observations is also very good for cloud liquid water path. However, the model seems to overestimate the CDNC over the 30° S–60° S latitude belt in summer. In general, these three cloud properties are simulated realistically by ECHAM5-HAMMOZ for the SH high latitudes.

3 Results and discussion

We now focus on the impact of ocean DMS on the cloud microphysics. For this, we analyze the CTRL and wo_ODMS simulations discussed in Sect. 2. Both the simulations are driven by same meteorological fields, so the differences in these runs (CTRL – wo_ODMS) are primarily due to the differences in the oceanic DMS emissions. The "simulated differences" are often defined as "anomalies" in this text.

3.1 Spatial and seasonal variations in the cloud microphysical properties

Here, we quantify the changes in the different processes outlined in Fig. 1 arising from the influence of DMS emissions. Gaseous phase H_2SO_4 is converted to sulfate particles, which in turn grows to cloud droplet size thereby modifying the cloud microphysical properties such as cloud droplet effective radii and the cloud cover. This will affect the atmospheric radiative forcing. The following sections discuss the DMS induced changes in the number of activated particles, CDNC, cloud droplet (CD) effective radii, cloud cover and the all sky radiative forcing at the top of the atmosphere in present day climate state.

3.1.1 Activated particles, CDNC, CD effective radii and total cloud cover

The number of particles available for activation to cloud droplets are termed activated particles and the change in the number of activated particles at 850 hPa is presented in Fig. 4. The figures show an increase in the number of activated particles in the CTRL simulation compared to the wo_ODMS case, especially over the southern belt (30° S–75° S) in the SH at 850 hPa during DJF 1999/2000 in the CTRL simulation compared to the wo_ODMS case. The maximum value of the anomalies is 2.7×10^8 per cubic meter over the 30° S–75° S latitudinal belt, with a mean value of 1.6×10^8 per cubic meter during the summer months. At 700 hPa, the activated particles are more prevalent in the 45° S–75° S belt (not shown here) with a maximum of up to 1.8×10^8 per cubic meter. A

ACPD
10, 3087–3127, 2010

significant contribution of DMS to the activated particles is also seen in MAM months at 850 hPa and is confined to a narrow belt around 30° S–45° S, but, the amplitude is half that of the DJF values. The seasonal cycle and spatial distribution of the particles available for activation follows the DMS emissions cycle and seasonality with a maximum during the SH summer months, gradually decreasing with a minimum during the SH winter months.

Figure 5 represents the seasonally averaged DMS related anomalies in CDNC burden for the simulation period. The anomalies show a clear seasonal cycle with four times higher mean concentrations of the cloud droplets in summer (DJF) than in the winter (June-July-August). The DMS related changes vary from 4×10^{10} 1/m^2 in summer to 1×10^{10} 1/m^2 in winter over the latitude belt 30° S–75° S. The zone of maximum CDNC anomaly is located in 40° S–75° S latitude belt in DJF and is shifted further north to 25° S–50° S in MAM months. The seasonal anomalies clearly follow the peak and variation of the ocean DMS emissions presented in Fig. 2.

Another source of aerosols (in addition to DMS emissions) that may contribute to the modification of the microphysical properties of clouds over the southern oceans is sea-salt aerosol. Studies have shown that sea-salt particles are a potential contributor to cloud condensation nuclei (Latham and Smith, 1990; Latham, 2002; Latham et al., 2008; Jones et al., 2009). However, as further discussed below, sea-salt derived CD number concentrations are relatively small in the southern high latitudes suggesting that DMS is the major contributor to cloud condensation nuclei, particularly, over the southern oceans during austral summer months.

The influence of ocean DMS emissions on the cloud top cloud droplet effective radius in microns is shown in Fig. 6. The effective radius is evaluated at the cloud top to facilitate comparison with the satellite data, that sees only the cloud top. This is computed from the difference between the two simulations (CTRL – wo_ODMS), and negative values, shown in blue, correspond to a decrease in the droplet radius with DMS generated sulfate aerosols in the atmosphere. There is a decrease in the droplet radius in summer (DJF) in the southern most latitude belt (30° S–75° S) in comparison

ACPD
10, 3087–3127, 2010

to the other regions. However, the decrease is not uniform along this belt and the values range from 0.5–2.0 µm, with a mean value of 0.73 µm. MODIS retrieved CD effective radii estimates show an average of ∼14 µm outside the phytoplankton bloom with a sharp decrease (to ∼10 µm) in the vicinity of the bloom (Meskhidze and Nenes, 2006). These estimates were taken from the southern ocean of an area averaged over 55° W–21° W and 42° S–60° S and gridded to a resolution of 2°×2°. This impact of DMS on cloud droplet effective radius is less prominent in the MAM months and is not seen in the other seasonal averages.

Increased number of small sized cloud droplets means less coalescence efficiency and hence, less precipitation thereby resulting in increased cloud lifetime (Albrecht, 1989; Ramaswamy et al., 2001; Lohmann and Feichter, 2005). This effect is also known as the cloud lifetime effect. The seasonally averaged anomalies of the total fraction covered by clouds is analyzed (Fig. A2). Positive values (in yellow) correspond to an increase in cloud cover in the CTRL simulation with DMS emissions. It is evident that there is an increase of the total cloud cover in the latitudinal band from 30° S–75° S in summer (DJF) of up to 6%. This increase in cloud coverage is shifted further north in the MAM months in consistence with the DMS emissions and the changes in CD number concentrations. The change in cloud cover is negligible during the rest of the year over the southern belt in the SH.

3.2 Aerosol radiative forcing at the top of the atmosphere

Aerosol radiative forcing is a perturbation evaluated as a difference between perturbed and unperturbed values of the radiative fluxes caused by aerosols calculated under the same meteorological conditions. Here, we evaluate the impact of the DMS induced changes at the top of the atmosphere (10 hPa). The radiative forcing is calculated as the difference between the net radiative flux at the TOA in the CTRL simulation and that in the wo_ODMS simulation under the same meteorological conditions. The large scale meteorology is constrained by nudging the fields to ERA40 reanalysis data, however, the small scale processes such as the aerosol-cloud feedback mechanisms are

enabled, thereby not strictly abiding by the definition of radiative forcing mentioned in IPCC (Forster et al., 2007). The global annual mean DMS related aerosol radiative forcing at the TOA in our model simulations is estimated as $-2.03\,W/m^2$. We are not aware of other studies evaluating this quantity, however, Gunson et al. (2006) evaluated the aerosol radiative forcing for doubling and halving ocean DMS scenarios as a difference of the radiative flux perturbation of the two DMS scenarios from their control simulation which included the present day ocean DMS. They obtained values of $2.0\,W/m^2$ and $-3.0\,W/m^2$ respectively.

The seasonal distribution of combined (shortwave+longwave) radiative forcing under all sky conditions is presented in Fig. 7. During the SH summer months (DJF), the radiative forcing is significantly lower reaching a minimum value of $-16\,W/m^2$ in the 30° S–75° S latitudinal belt coinciding with the increased DMS emissions during these months. The simulated changes in the TOA radiative forcing are consistent with those calculated from satellite data presented in Meskhidze and Nenes (2006) where very strong cooling reaching $-15\,W/m^2$ is estimated in the biologically active regions in the southern oceans. The region of strong cooling (maximum negative radiative forcing belt) is shifted further north to 25° S–50° S latitude belt during SH spring and autumn where values range from -1 to $-7\,W/m^2$. The forcing is less than $-1\,W/m^2$ in SH winter.

3.3 Temporal variability in cloud microphysical properties

Here, we quantify the contribution of DMS to the changes in the cloud microphysical properties over the southern oceans. We consider three Southern Hemisphere latitudinal bands to facilitate comparison with the study by Korhonen et al. (2008): 30° S–45° S, 45° S–60° S, 60° S–75° S. The DMS derived changes in the number of activated particles and CDNC burden in these latitudinal bands are presented in Figs. 8 and 9, respectively.

Figure 8 shows the temporal distribution of the number of activated aerosol particles at 850 hPa per cubic meter in the three latitude bands. The seasonal variation in the

CTRL run (black line) that includes the DMS emissions is simulated in consistence with the ocean DMS seasonal cycle in all the 3 latitude bands with a maximum during the SH summer months and a minimum during the SH winter. The magnitude is two times higher than in the wo_ODMS simulation (red line), especially over the SH summer months. This implies that the DMS derived activated particles are significantly higher in the 45° S–75° S latitude belt during these months of the year compared to particles derived from other sources. However, there is a slight increase in the number of activated aerosol particles northward of 45° S in the wo_ODMS run which may be due to the particles from other sources.

Zonally averaged time series of the simulated CDNC burden for the three latitude bands are presented in Fig. 9. The black line and the red line show the absolute values of the cloud droplet concentrations in the CTRL simulation and the wo_ODMS simulation respectively. The seasonal variation in the vertically integrated CD number concentrations is evident south of 45° S in the CTRL simulation (black line). As in the case of Fig. 8, the CDNC burden in the wo_ODMS run (red line) also does not show a seasonal variation, but, remains constant at around 0.2×10^{11} 1/m^2 in the 30° S–60° S and around 0.1×10^{11} 1/m^2 beyond 60° S. The amplitude is twice as high in the CTRL simulation in comparison to the wo_ODMS run during the summer in the 30° S–75° S latitude belt. The CDNC burden reaches as high as 0.6×10^{11} 1/m^2 during the austral summer months coinciding with the intense biological productivity during this season.

The DMS derived contribution to the CDNC burden in the three latitude belts averaged over the austral summer months is presented in Table 2 as percentage deviations with respect to the wo_ODMS simulation. Our study shows an increase in the number of cloud droplets when ocean DMS is included. The mean increase in CDNC burden is 128% in the CTRL simulations when averaged over the DJF months in the 30° S–75° S latitude belt. The maximum increase is seen in the southern most belt (60° S–75° S) in the SH, where the mean CDNC burden increases by 176% with respect to the simulation when the ocean DMS is switched off. More than 100% increase in the CDNCs are seen in the 45° S–60° S belt and the percentage increase is comparatively lower (89%)

ACPD
10, 3087–3127, 2010

in the 30° S–45° S belt. We compare our results to the study of Korhonen et al. (2008) who used an offline global chemistry transport model to evaluate the DMS contribution to cloud condensation nuclei in a similar experimental set up. Their simulation obtained a 46% increase in the CCN burden in January in the 30° S–45° S belt which is lower compared to our results. However, the percentage changes in the latitudinal belt 45° S–75° S is even smaller (11–18% at 45° S–60° S and 40% at 60° S–75° S) in the study of Korhonen et al. (2008) compared to our results. They attribute this to the high sea spray contribution to CCN at these latitudes in their model and also, to the entrainment of the CCN into the marine boundary layer from the summer time free troposphere from distant continental sources when the ocean DMS is switched off. Meskhidze and Nenes (2006) estimated the monthly averaged CDNC outside the bloom and compared them with that inside the phytoplankton bloom area (48° S–56° S) in the southern oceans and showed that the cloud droplet number was doubled.

The changes in the CD effective radii in percentage due to the DMS perturbation are presented in Table 3 for the SH summer months. The percentage differences show negative values during the SH summer months, meaning smaller droplet size in the CTRL simulation in comparison to the wo_ODMS experiment. This may be due to the fact that in the CTRL simulation, we have more aerosols competing for the available water vapour that is a constant in both the simulations, thereby resulting in a decrease in the droplet size compared to when the DMS derived aerosols are not present. The droplet radius is smaller by up to 7.4% in the southern most belt in the SH and by about 6.5% north of 60° S during DJF 1999/2000. The mean decrease in the droplet radius is 6% when averaged over the 30° S–75° S latitude belt in austral summer. Analysis of the satellite data indicates a decrease of 20–25% in the cloud droplet radius inside the phytoplankton bloom regions in the southern oceans (Meskhidze and Nenes, 2006). The maximum decrease observed in our simulations over the southern oceans is 15–18%.

The DMS induced contribution to cloud cover is presented in Table 4. Cloud cover is greater in the CTRL simulation in comparison to the wo_ODMS run in the three

ACPD
10, 3087–3127, 2010

SH latitude bands during the austral summer. The mean total cloud cover increases by 3.5% in the northern most belt (30° S–45° S), and by approximately 1.7% in the latitudinal belts south of 45° S.

4 Conclusions

In this paper we quantify the DMS derived changes in the cloud microphysical properties. These changes are evaluated over the southern oceans (30° S–75° S) where anthropogenic effects are minimal. Our main focus is during the austral summer, when the DMS flux to the atmosphere is high. We also present the spatial and seasonal averages for the rest of the year. To assess this, the state of the art, ECHAM5-HAMMOZ general circulation model that has a detailed aerosol module coupled to detailed chemistry and cloud microphysics modules is used. Two experiments are carried out: (1) a baseline simulation that includes the ocean DMS emissions (CTRL) and (2) a simulation in which the ocean DMS emissions are turned off (wo_ODMS). The difference between these two simulations represents the contribution from the ocean DMS emissions.

The main findings of our simulations are summarized below:

1. Our simulations show a clear seasonality in the variation in DMS derived aerosol particles over the southern oceans which mirror the changes in biological activity over the year in consistent with the earlier studies by Boers et al. (1996, 1998); Ayers and Gillett (2000); Meskhidze and Nenes (2006).

2. The simulated global annual mean DMS flux to the atmosphere is 23.3 Tg(S)/yr, is in good agreement with Boucher et al. (2003) study based on similar parameterization scheme.

3. The DMS derived CDNC contributes to about 128% averaged over the 30° S–75° S latitude belt during the SH summer months. However, this estimate is

ACPD
10, 3087–3127, 2010

overestimated when compared to the CCN burden estimates by Korhonen et al. (2008). Over the 30° S–75° S latitudinal belt, the CTRL simulation demonstrates seasonality in DMS derived CDNC with a maximum during austral summer and a minimum during the winter, whereas the simulated CDNC in the wo_ODMS experiment do not show this seasonality.

4. The evaluation of the wo_ODMS simulation in the northern most latitude belt (30° S–45° S) analyzed in this study indicates the presence of CDNC derived from other sources such as, seasalt, but is negligible compared to the DMS contribution to CDNC, particularly, in SH summer.

5. Our simulations also reproduce an increased number of smaller sized cloud droplets during austral summer and autumn in the 30° S–60° S latitude band. Vertically integrated atmospheric water vapour is held constant in the two simulations, thus, this is a demonstration of the first aerosol indirect effect. The maximum decrease in our model derived droplet radius is 15–18% compared to the 20–25% decrease estimated from MODIS derived estimates published in Meskhidze and Nenes (2006).

6. DMS emissions increase the simulated cloud cover by about 3.5% in the 30° S–45° S belt, by around 1.7% in the 45° S–75° S belt during the SH summer months.

7. The radiative forcing due to DMS derived sulfate aerosols reaches a minimum value of $-16\,W/m^2$ in the 30° S–75° S latitude belt in the DJF averages. This is in agreement with Meskhidze and Nenes (2006) study where strong cooling reaching $-15\,W/m^2$ in the biologically productive regions is found. The global annual mean indirect aerosol radiative forcing due to DMS is $-2.03\,W/m^2$.

The CLAW hypothesis was postulated as a fundamental climate feedback. However, the research since then has helped us understand the complexities in the different processes involved and the difficulties in assessing the strength of the feedback. Uncertainties still exist in the quantification of the influence of DMS on climate in a future

ACPD
10, 3087–3127, 2010

climate scenario. For example, recent works (Yoon and Brimblecombe, 2002; Pierce and Adams, 2006; Smith, 2007) have shown that the sea salt aerosols play a major role in marine CCN production, thereby affecting the albedo and lifetime of clouds. Further research is required to quantify the relative roles of sea salt and DMS in marine CCN production over the southern oceans.

Appendix A

See Figs. A1 and A2.

Acknowledgements. This work was supported and funded by the QUEST-feedbacks project under the UK Natural Environment Research Council (NERC) QUEST programme. We acknowledge the availability of HOAPS-3 data from the World Data Center for Climate at DKRZ, Hamburg, Germany. AD would like to thank Andrew Heidinger (NOAA/NESDIS) for providing PATMOS-x data.

References

Albrecht, B.: Aerosols, Cloud Microphysics, and Fractional Cloudiness, Science, 245, 1227–1230, 1989. 3100

Andersson, A., Bakan, S., Karsten, F., Grassl, H., Klepp, C.-P., and Schulz, J.: Hamburg Ocean Atmosphere Parameters and Fluxes from Satellite Data – HOAPS-3-monthly mean, World Data Center for Climate, 2007. 3097

Andreae, M. O., Wolfgang, E., and de Mora, S.: Biogenic sulfur emissions and aerosols over the tropical South Atlantic 3. Atmospheric dimethylsulfide, aerosols and cloud condensation nuclei, J. Geophys. Res., 100, 11335–11356, 1995. 3089

Auvray, M., Bey, I., Llull, E., Schultz, M. G., and Rast, S.: A model investigation of tropospheric ozone chemical tendencies in long-range transported pollution plumes, J. Geophys. Res., 112, D05304, doi:10.1029/2006JD007137, 2007. 3094

Ayers, G. and Gras, J.: Seasonal relationships between cloud condensation nuclei and aerosol methane sulphonate in marine air, Nature, 353, 834–835, 1991. 3089

Ayers, G. P. and Gillett, R. W.: DMS and its oxidation products in the remote marine atmosphere: implications for climate and atmospheric chemistry, J. Sea Res., 43, 275–286, 2000. 3096, 3104

Bates, T. S. and Quinn, P. K.: Dimethylsulfide (DMS) in the equatorial Pacific Ocean (1982 to 1996): Evidence of a climate feedback?, Geophys. Res. Lett., 24, 861–864, 1997. 3090

Bates, T. S., Cline, J. D., Gammon, R. H., and Kelly-Hanse, S. R.: Regional and seasonal variations in the flux of oceanic Dimethylsulfide to the atmosphere, J. Geophys. Res., 92, 2930–2938, 1987. 3090

Boers, R., Ayers, G., and Gras, J.: Coherence between seasonal variation in satellite-derived cloud optical depth and boundary layer CCN concentrations at a mid-latitude Southern Hemisphere station, Tellus, 46B, 123–131, 1994. 3089

Boers, R., Jensen, J. B., Krummel, P. B., and Gerber, H.: Microphysical and short-wave radiative structure of wintertime stratocumulus clouds over the Southern Ocean, Q. J. Roy. Meteorol. Soc., 122, 1307–1339, 1996. 3096, 3104

Boers, R., Jensen, J. B., and Krummel, P. B.: Microphysical and short-wave radiative structure of stratocumulus clouds over the Southern Ocean: Summer results and seasonal differences, Q. J. Roy. Meteorol. Soc., 124, 151–168, 1998. 3096, 3104

Boucher, O., Moulin, C., Belviso, S., Aumont, O., Bopp, L., Cosme, E., von Kuhlmann, R., Lawrence, M. G., Pham, M., Reddy, M. S., Sciare, J., and Venkataraman, C.: DMS atmospheric concentrations and sulphate aerosol indirect radiative forcing: a sensitivity study to the DMS source representation and oxidation, Atmos. Chem. Phys., 3, 49–65, 2003, http://www.atmos-chem-phys.net/3/49/2003/. 3096, 3104

Charlson, R. J., Lovelock, J. E., Andreae, M. O., and Warren, S. G.: Oceanic phytoplankton, atmospheric sulphur, cloud albedo and climate, Nature, 326, 655–661, 1987. 3089

Feichter, J., Kjellstrom, E., Rodhe, H., Dentener, F., Lelieveld, J., and Roelofs, G.: Simulation of the tropospheric sulfur cycle in a global climate model, Atmos. Environ., 30, 1693–1707, 1996. 3093

Forster, P., Ramaswamy, V., Artaxo, P., Berntsen, T., Betts, R., Fahey, D., Haywood, J., Lean, J., Lowe, D., Myhre, G., Nganga, J., Prinn, R., Raga, G., Schulz, M., and Dorland, R. V.: Changes in Atmospheric Constituents and in Radiative Forcing, in: Climate Change 2007: The Physical Science Basis. Contribution of Working Group I to the Fourth Assessment Report of the Intergovernmental Panel on Climate Change, edited by: Solomon, S., Qin, D., Manning, M., Chen, Z., Marquis, M., Averyt, K. B., Tignor, M., and Miller, H. L., Cambridge

University Press, Cambridge, United Kingdom and New York, NY, USA, 2007. 3101
Gondwe, M., Krol, M., Gieskes, W., Klaassen, W., and de Baar, H.: The contribution of ocean-leaving DMS to the global atmospheric burdens of DMS, MSA, SO_2, and nssSO_4=, Global Biogeochem. Cy., 17(2), 1056, doi:10.1029/2002GB001937, 2003. 3091, 3097
Gunson, J. R., Spall, S. A., Anderson, T. R., Jones, A., Totterdell, I. J., and Woodage, M. J.: Climate sensitivity to ocean dimethylsulphide emissions, Geophys. Res. Lett., 33, L07701, doi:10.1029/2005GL024982, 2006. 3090, 3101
Hegg, D., Radke, L., and Hobbs, P.: Measurements of Aitken nuclei and cloud condensation nuclei in the marine atmosphere and their relationship to the DMS-cloudclimate hypothesis, J. Geophys. Res., 96, 18727–18733, 1991. 3089
Horowitz, L. W., Walters, S., Mauzerall, D. L., Emmons, L. K., Rasch, P. J., Granier, C., Tie, X., Lamarque, J., Schultz, M. G., Tyndall, G. S., Orlando, J. J., and Brasseur, G. P.: A global simulation of tropospheric ozone and related tracers: Description and evaluation of MOZART, version 2, J. Geophys. Res., 108(D24), 4784, doi:10.1029/2002JD002853, 2003. 3092
Jones, A., Haywood, J., and Boucher, O.: Climate impacts of geoengineering marine stratocumulus clouds, J. Geophys. Res., 114, D10106, doi:10.1029/2008JD011450, 2009. 3099
Kettle, A. and Andreae, M.: Flux of dimethylsulfide from the oceans: A comparison of updated data sets and flux models, J. Geophys. Res., 105, 26793–26808, 2000. 3092, 3096
Kettle, A. J., Andreae, M. . O., Amourou, D., Andreae, T. W., Bates, T. S., Berresheim, H., ingemer, H. B., Boniforti, R., Curran, M., DiTullio, G. R., Helas, G., Jones, G. B., Keller, M. D., Kiene, R. P., Leck, C., Levasseur, M., Malin, G., Maspero, M., Matrai, P., McTaggart, A. R., Mihalopoulos, N., Nguyen, B., Novo, A., J.P.Putaud, Rapsomanikis, S., Roberts, G., Schebeske, G., Sharma, S., Simo, R., Staubes, R., Turner, S., and Uher, G.: A global database of sea surface dimethylsulfide (DMS) measurements and a procedure to predict sea surface D MS as a function of latitude, longitude, and month, Global Biogeochem. Cy., 13, 399–444, 1999. 3092
Kloster, S., Feichter, J., Maier-Reimer, E., Six, K. D., Stier, P., and Wetzel, P.: DMS cycle in the marine ocean-atmosphere system – a global model study, Biogeosciences, 3, 29–51, 2006, http://www.biogeosciences.net/3/29/2006/. 3091
Kloster, S., Feichter, J., Maier-Reimer, E., Roeckner, E., Stier, P., Wetzel, P., Six, K. D., and Esch, M.: Response of DMS in the ocean and atmosphere to global warming, J. Geophys. Res.-Biogeosciences, 112, G03005, doi:10.1029/2006JG000224, 2007. 3090
Korhonen, H., Carslaw, K., Spracklen, D., Mann, G., and Woodhouse, M.: Influence

of oceanic DMS emissions on CCN concentrations and seasonality over the remote southern hemisphere oceans: A global model study, J. Geophys. Res., 113, D15204, doi:10.1029/2007JD009718, 2008. 3089, 3091, 3101, 3103, 3105

Latham, J.: Amelioration of global warming by controlled enhancement of the albedo and longevity of low-level maritime clouds, Atmos. Sci. Lett., 3, 52–58, 2002. 3099

Latham, J. and Smith, M.: Effect on global warming of wind-dependent aerosol generation at the ocean surface, Nature, 347, 372–373, 1990. 3099

Latham, J., Rasch, P., Chen, C., Kettles, L., Gadian, A., Gettelman, A., Morrison, H., Bower, K., and Choularton, T.: Global temperature stabilization via controlled albedo enhancement of low-level maritime clouds, Philos. T. Roy. Soc. A, 366, 3969–3987, 2008. 3099

Leck, C., Larsson, U., Baegander, L. E., Johansson, S., and Hajdu, S.: DimethylSulfide in the Baltic Sea: Annual variability in relation to biological activity, J. Geophys. Res., 95, 3353–3363, 1990. 3090

Lohmann, U. and Feichter, J.: Global indirect aerosol effects: a review, Atmos. Chem. Phys., 5, 715–737, 2005, http://www.atmos-chem-phys.net/5/715/2005/. 3100

Lohmann, U. and Roeckner, E.: Design and performance of a new cloud microphysics scheme developed for the ECHAM general circulation model, Clim. Dynam., 12(8), 557–572, 1996. 3093

Lohmann, U., Feichter, J., Chuang, C. C., and Penner, J. E.: Predicting the number of cloud droplets in the ECHAM GCM, J. Geophys. Res., 104, 9169–9198, 1999. 3092, 3094, 3097

Lohmann, U., Stier, P., Hoose, C., Ferrachat, S., Kloster, S., Roeckner, E., and Zhang, J.: Cloud microphysics and aerosol indirect effects in the global climate model ECHAM5-HAM, Atmos. Chem. Phys., 7, 3425–3446, 2007, http://www.atmos-chem-phys.net/7/3425/2007/. 3092, 3094

Machenhauer, B. and Kirchner, I.: Diagnosis of systematic initial tendency errors in the ECHAM AGCM using slow normal mode data assimilation of ECMWF reanalysis data, CLIVAR Exchanges, 5, 9–10, 2000. 3093

Meskhidze, N. and Nenes, A.: Phytoplankton and cloudiness in the Southern Ocean, Science, 314, 1419–1423, 2006. 3090, 3096, 3100, 3101, 3103, 3104, 3105

Nightingale, P. D., Malin, G., Law, C. S., Liss, A. J. W. P. S., Liddicoat, M. I., Boutin, J., and Upstill-Goddard, R. C.: In situ evaluation of air-sea gas exchange parameterizations using novel conservative and volatile tracers, Global Biogeochem. Cy., 14, 373–388, 2000. 3093,

3096
O'Dowd, C. D., Lowe, J. A., Smith, M. H., Davison, B., Hewitt, C. N., and Harrison, R. M.: Biogenic sulphur emissions and inferred non-sea-salt-sulphate cloud condensation nuclei in and around Antarctica, J. Geophys. Res., 102(D11), 12839–12854, 1997. 3089
Pierce, J. R. and Adams, P. J.: Global evaluation of CCN formation by direct emission of sea salt and growth of ultrafine sea salt, J. Geophys. Res., 111, D06203, doi:10.1029/2005JD006186, 2006. 3106
Pozzoli, L.: Climate and chemistry interactions: Develpoment and evaluation of a coupled chemistry-aerosol-climate model, Ph.D. thesis, Ecole Polytech. Fed. de Lausanne, Lausanne, Switzerland, 2007. 3094
Pozzoli, L., Bey, I., Rast, J. S., Schultz, M. G., Stier, P., and Feichter, J.: Trace gas and aerosol interactions in the fully coupled model of aerosol-chemistry-climate ECHAM5-HAMMOZ: 1. Model description and insights from the spring 2001 TRACE-P experiment, J. Geophys. Res., 113, D07308, doi:10.1029/2007JD009007, 2008a. 3092
Pozzoli, L., Bey, I., Rast, J. S., Schultz, M. G., Stier, P., and Feichter, J.: Trace gas and aerosol interactions in the fully coupled model of aerosol-chemistry-climate ECHAM5-HAMMOZ: 2. Impact of heterogeneous chemistry on the global aerosol distributions, J. Geophys. Res., 113, D07309, doi:10.1029/2007JD009008, 2008b. 3095
Quaas, J., Boucher, O., and Lohmann, U.: Constraining the total aerosol indirect effect in the LMDZ and ECHAM4 GCMs using MODIS satellite data, Atmos. Chem. Phys., 6, 947–955, 2006, http://www.atmos-chem-phys.net/6/947/2006/. 3097
Ramaswamy, V., Boucher, O., Haigh, J., Hauglustaine, D., Haywood, J., Myhre, G., Nakajima, T., Shi, G. Y., and Solomon, S.: Radiative Forcing of Climate Change, in: Climate Change 2001: The Scientific Basis, Contribution of working group I to the Third Assessment Report of the Intergovernmental Panel on Climate Change, edited by: Houghton, J. T., Ding, Y., Griggs, D. J., et al., Cambridge University Press, New York, 349–416, 2001. 3100
Rast, S., Schultz, M. G., Bey, I., van Noije, T., Aghedo, A. M., Brasseur, G. P., Diehl, T., Esch, M., Ganzeveld, L., Kirchner, I., Kornblueh, L., Rhodin, A., Roeckner, E., Schmidt, H., Schroeder, S., Schulzweida, U., Stier, P., Thomas, K., and Walters, S.: Evaluation of the tropospheric chemistry general circulation model ECHAM5-MOZ and its application to the analysis of interannual variability in tropospheric ozone from 1960–2000, J. Geophys. Res., in review, 2010. 3094

Reade, L., Jennings, S. G., and McSweeney, G.: Cloud condensation nuclei measurements at Mace Head, Ireland, over the period 1994–2002, Atmos. Res., 82, 610–621, 2006. 3090
Roeckner, E., Baeuml, G., Bonventura, L., Brokopf, R., Esch, M., Giorgetta, M., Hagemann, S., Kirchner, I., Kornblueh, L., Manzini, E., Rhodin, A., Schlese, U., Schulzweida, U., and Tompkins, A.: The atmospheric general circulation model ECHAM5. PART I: Model description,, MPI-Report, 349, 127 pp., 2003. 3092
Schulz, M., de Leeuw, G., and Balkanski, Y.: Sea-salt aerosol source functions and emissions, in Emissions of Atmospheric Trace Compounds, Springer, New York, 333–359, 2004. 3092
Smith, M. H.: Sea-salt particles and the CLAW hypothesis, Environ. Chem., 4(6), 391–395, 2007. 3106
Stier, P., Feichter, J., Kinne, S., Kloster, S., Vignati, E., Wilson, J., Ganzeveld, L., Tegen, I., Werner, M., Balkanski, Y., Schulz, M., Boucher, O., Minikin, A., and Petzold, A.: The aerosol-climate model ECHAM5-HAM, Atmos. Chem. Phys., 5, 1125–1156, 2005, http://www.atmos-chem-phys.net/5/1125/2005/. 3092, 3093, 3094, 3095
Tegen, I., Harrison, S. P., Kohfeld, K., I. C. Prentice, M. C., and Heimann, M.: Impact of vegetation and preferential source areas on global dust aerosol: Results from a model study, J. Geophys. Res., 107(D21), 4576, doi:10.1029/2001JD000963, 2002. 3092
Uppala, S., Kallberg, P., Simmons, A., Andrae, U., da Costa Bechtold, V., Fiorino, M., Gibson, J., Haseler, J., Hernandez, A., Kelly, G., Li, X., Onogi, K., Saarinen, S., Sokka, N., Allan, R. P., Andersson, E., Arpe, K., Balmaseda, M., Beljaars, A., van de Berg, L., Bidlot, J., Bormann, N. ., Caires, S., Chevallier, F., Dethof, A., Dragosavac, M., Fisher, M., Fuentes, M., nn, S. H., Holm, E., Hoskins, B., Isaksen, L., Janssen, P., Jenne, R., McNally, A. P., Mahfouf, J.-F., Morcrette, J.-J., Rayner, N., Saunders, R., Simon, P., Sterl, A., Trenberth, K. E., Untch, A., Vasiljevic, D., Viterbo, P., and Woollen, J.: The ERA-40 re-analysis, Q. J. Roy. Meteorol. Soc., 131, 2961–3012, 2005. 3093
Vallina, S. M. and Simo, R.: Strong relationship between DMS and the solar radiation dose over the global surface ocean, Science, 315, 506–508, 2007. 3090
Woodhouse, M. T., Mann, G. W., Carslaw, K. S., and Boucher, O.: New Directions: The impact of oceanic iron fertilisation on cloud condensation nuclei, Atmos. Environ., 42, 5728–5730, 2008. 3091
Yoon, Y. J. and Brimblecombe, P.: Modelling the contribution of sea salt and dimethyl sulfide derived aerosol to marine CCN, Atmos. Chem. Phys., 2, 17–30, 2002, http://www.atmos-chem-phys.net/2/17/2002/. 3106

Yum, S. S. and Hudson, J. G.: Wintertime/summertime contrasts of cloud condensation nuclei and cloud microphysics over the Southern Ocean, J. Geophys. Res., 109, D06204, doi:10.1029/2003JD003864, 2004. 3089

Table 1. Comparison of CD effective radii, CDNC and cloud liquid water path Cloud LWP) averaged over 30S-60S for DJF 1999/2000 from both model simulations and satellite observations. The HOAPS cloud liquid water path data are available only over ocean, hence, the averages are taken over ocean only.

Parameters	Satellite data	Model
CD effective radii (μm)	11.61	11.39
CDNC ($1/m^2$)	3.4×10^{10}	4.4×10^{10}
Cloud LWP (kg/m^2)	0.095	0.0925

Table 2. Percentage mean change (calculated as [(CTRL – wo_ODMS)/wo_ODMS]·100) in the zonally averaged CDNC burden over the given latitudinal belts for the period December 1999–March 2000.

Lat. ⇓ // Mon. ⇒	December	January	February	March
45° S–30° S	70.2	87.8	109.6	97.3
60° S–45° S	119.6	118.9	116.2	73.6
75° S–60° S	214.7	191.2	120.8	65.3

Table 3. Percentage mean change (calculated as [(CTRL – wo_ODMS)/wo_ODMS]·100) in the zonally averaged cloud top cloud droplet effective radii over the given latitudinal belts for the period December 1999–March 2000.

Lat. ⇓ // Mon. ⇒	December	January	February	March
45° S–30° S	−5.81	−6.07	−6.41	−5.90
60° S–45° S	−6.78	−6.00	−6.15	−5.63
75° S–60° S	−7.44	−5.14	−3.78	−1.10

Table 4. Percentage mean change (calculated as [(CTRL – wo_ODMS)/wo_ODMS]·100) in the zonally averaged total cloud cover over the given latitudinal belts for the period December 1999–March 2000.

Lat. ⇓ // Mon. ⇒	December	January	February	March
45° S–30° S	2.70	3.41	4.23	4.20
60° S–45° S	1.88	2.19	1.91	1.50
75° S–60° S	1.55	1.19	1.26	1.04

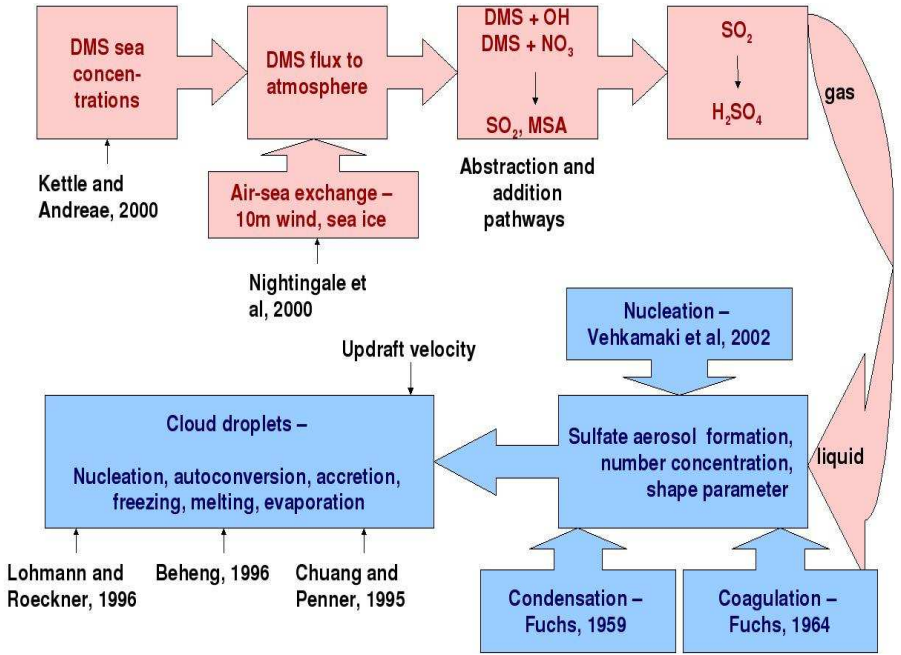

Fig. 1. Schematic showing the processes from DMS flux to the atmosphere to the cloud droplets as represented in the ECHAM5-HAMMOZ model.

ACPD
10, 3087–3127, 2010

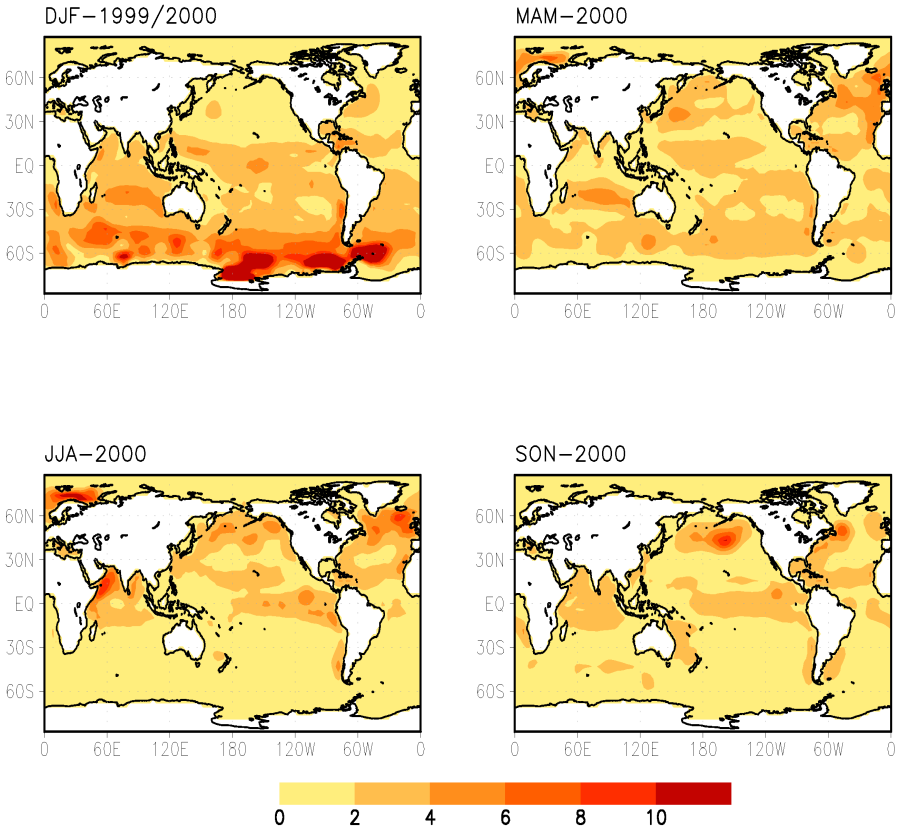

Fig. 2. Seasonal averages of ocean DMS emissions in Kg(S)/m^2/s (multiplied by 10^{12}).

ACPD
10, 3087–3127, 2010

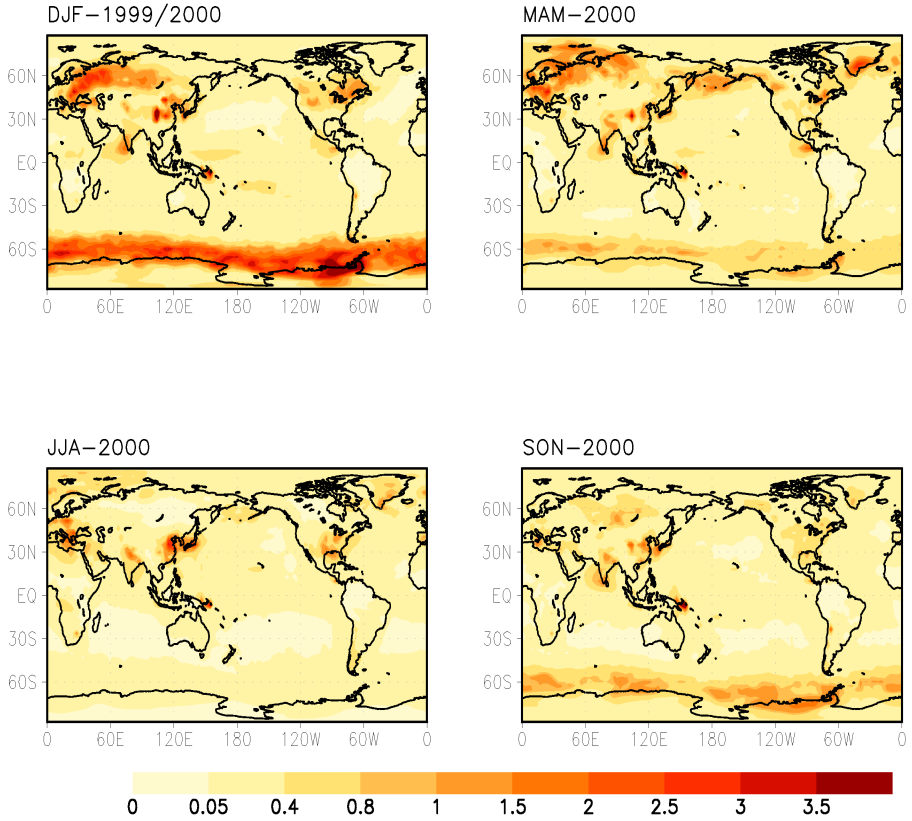

Fig. 3. Seasonal averages of H_2SO_4 concentrations in mass mixing ratios (MMR) at 850 hPa (multiplied by 10^{12}).

ACPD
10, 3087–3127, 2010

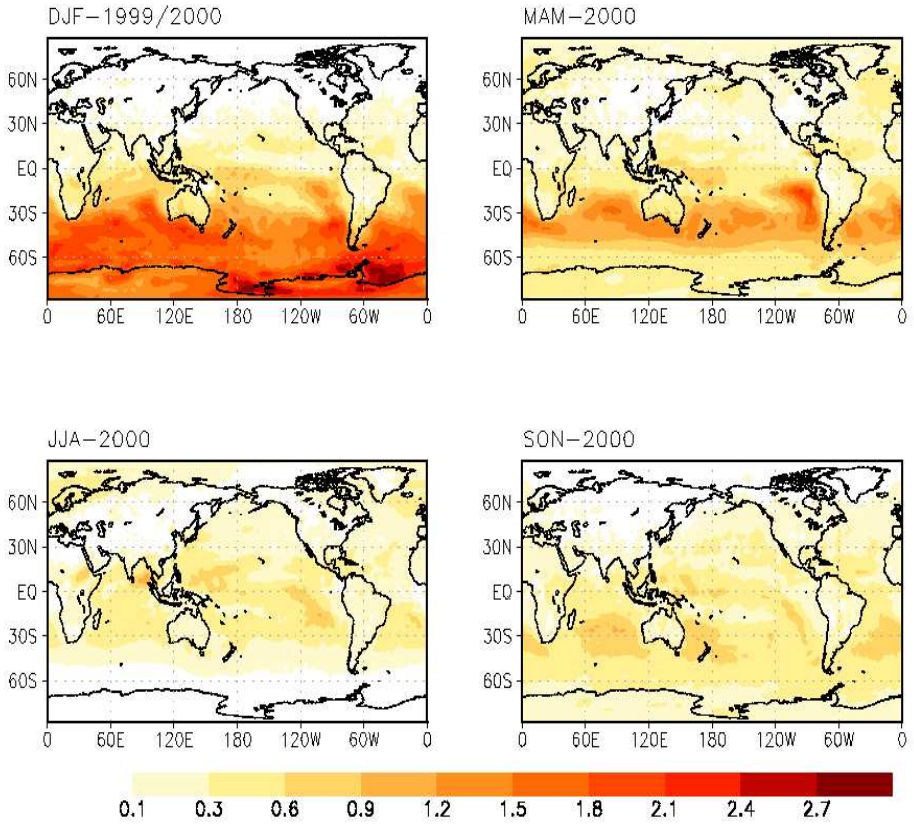

Fig. 4. Seasonal averages of changes in the number of activated particles at 850 hPa ($1/m^3$) in the CTRL simulation compared to the wo_ODMS simulation (multiplied by 10^{-8}). Positive values mean there is an increase in the number of activated particles in the simulation when the DMS sea water concentrations are present.

ACPD
10, 3087–3127, 2010

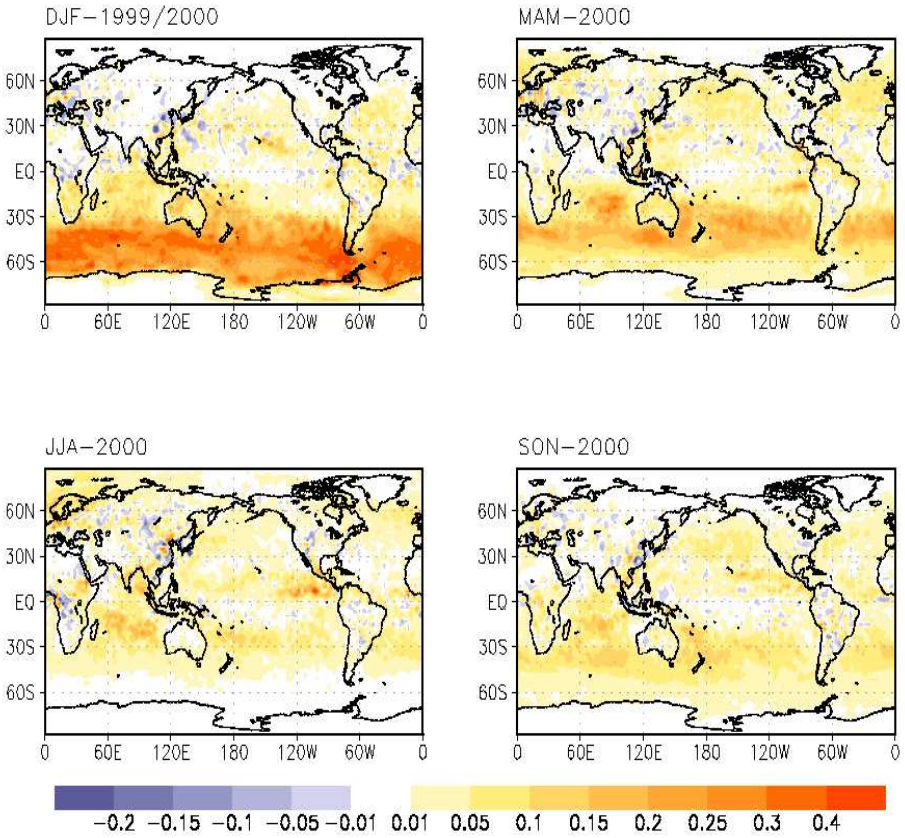

Fig. 5. Seasonal averages of changes in the vertically integrated cloud droplet number concentration (CDNC) ($1/m^2$) in the CTRL simulation compared to the wo_ODMS simulation (multiplied by 10^{-11}). Positive values mean there is an increase in CDNCs in the simulation when the DMS sea water concentrations are present.

ACPD
10, 3087–3127, 2010

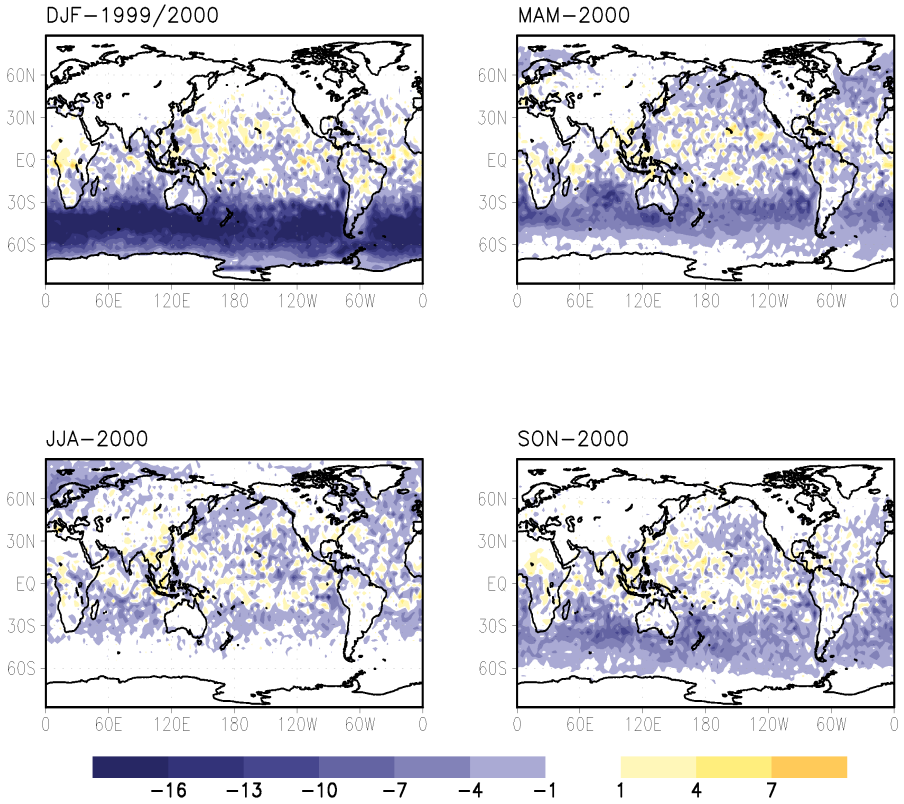

Fig. 6. Seasonal averages of changes in the cloud top cloud droplet effective radii(μm) in the CTRL simulation compared to the wo_ODMS simulation. Negative values mean there is a decrease in CD radius in the simulation when the DMS sea water concentrations are present.

ACPD
10, 3087–3127, 2010

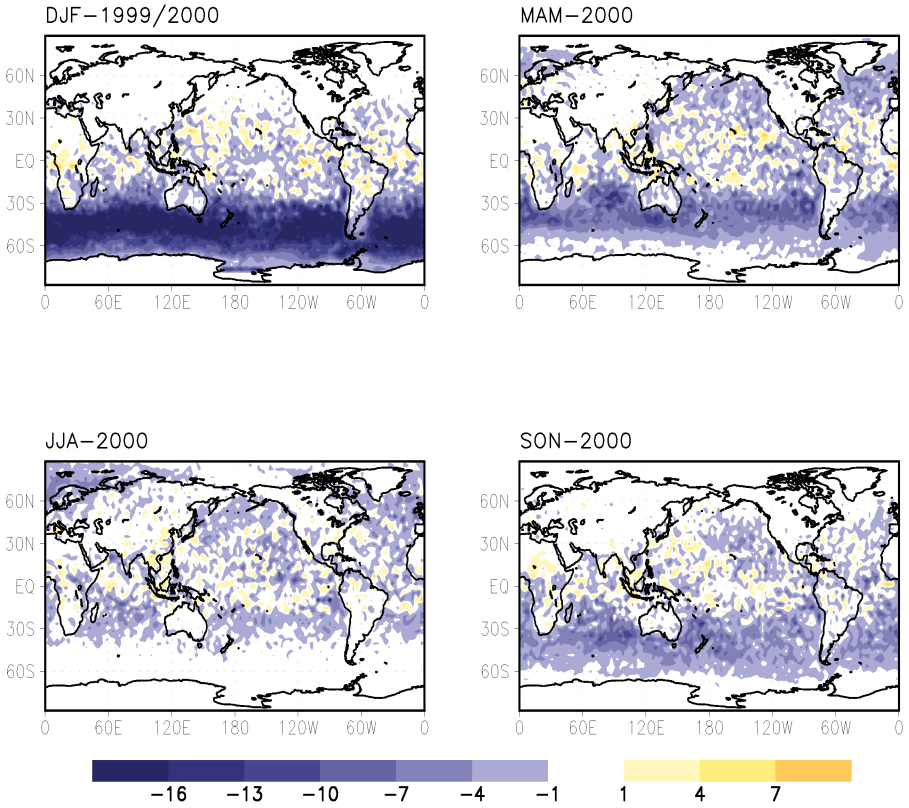

Fig. 7. Seasonal averages of total sky aerosol radiative forcing at the TOA (W/m^2). Negative aerosol radiative forcing means there is a net cooling at the TOA.

ACPD
10, 3087–3127, 2010

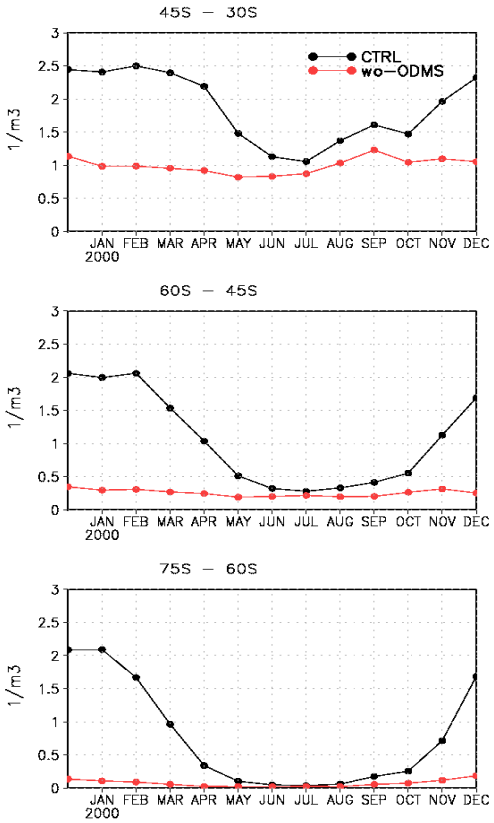

Fig. 8. Latitudinally averaged time series (December 1999–December 2000) of the number of activated particles at 850 hPa ($1/m^3$) (multiplied by 10^{-8}) shown as absolute values in **(a)** CTRL simulation denoted by the black line **(b)** wo_ODMS simulation denoted by the blue line.

ACPD
10, 3087–3127, 2010

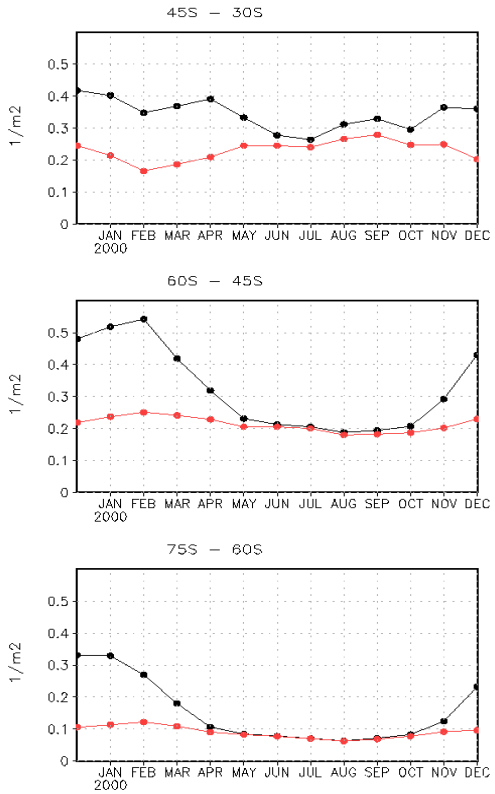

Fig. 9. Latitudinally averaged time series (December 1999–December 2000) of the CDNC burden ($1/m^2$) (multiplied by 10^{-11}) shown as absolute values in **(a)** CTRL simulation denoted by the black line **(b)** wo_ODMS simulation denoted by the blue line.

ACPD
10, 3087–3127, 2010

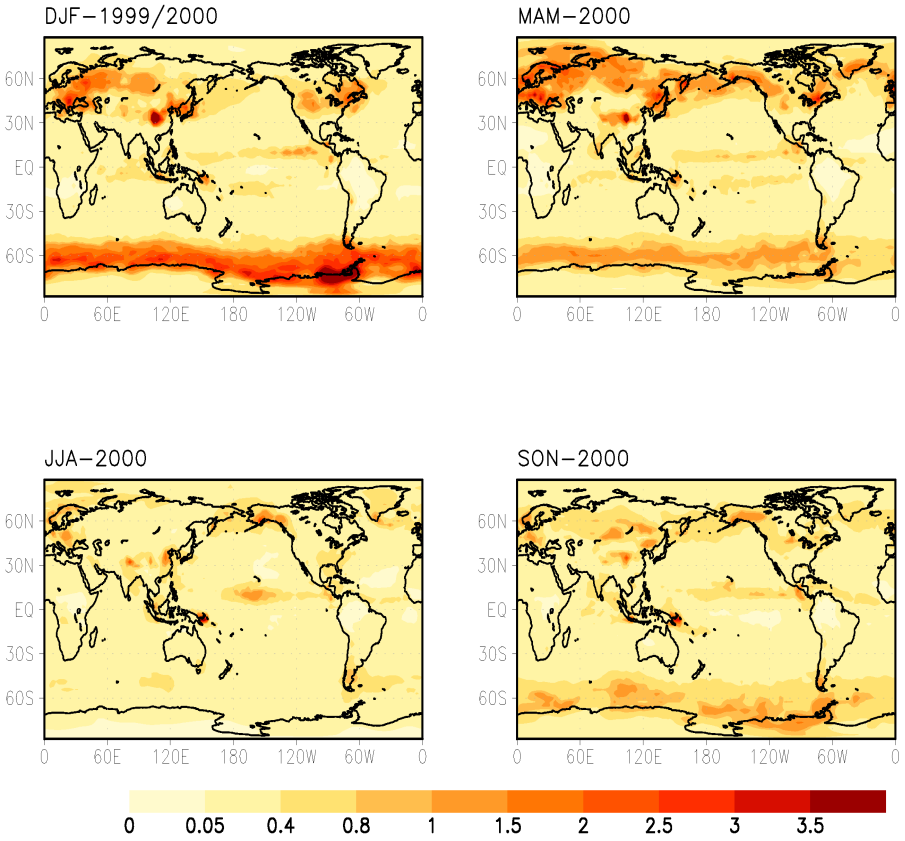

Fig. A1. Seasonal averages of H_2SO_4 concentrations in mass mixing ratios (MMR) at 700 hPa (multiplied by 10^{12}).

ACPD
10, 3087–3127, 2010

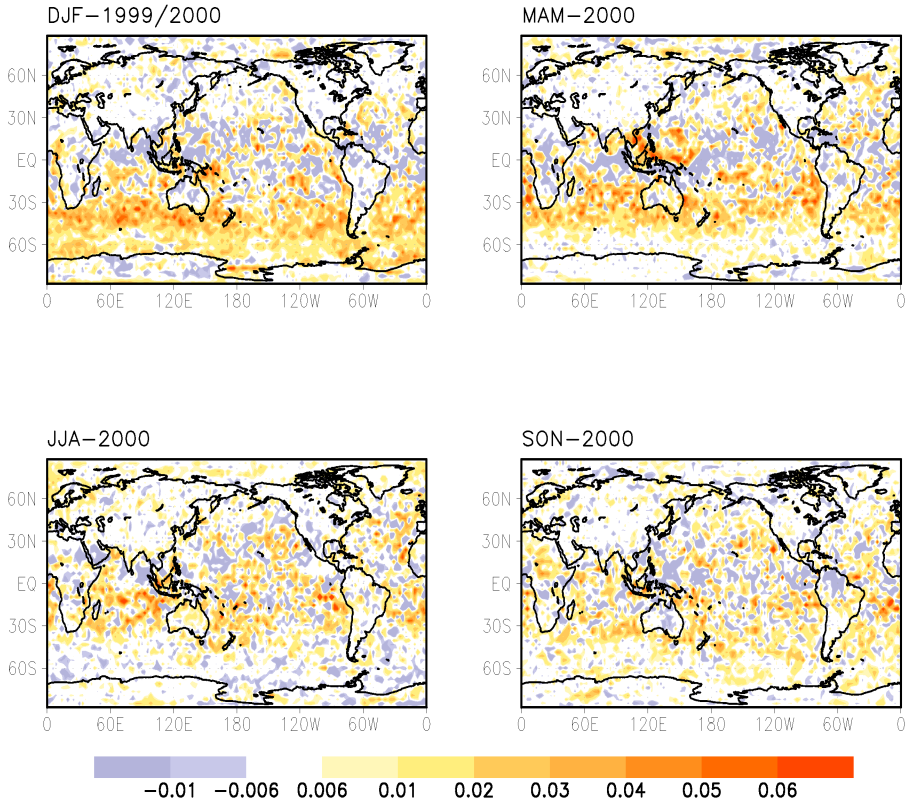

Fig. A2. Seasonal changes in the total cloud cover fraction in the CTRL simulation compared to the wo_ODMS simulation. Positive values mean there is an increase in cloud cover in the simulation when the DMS sea water concentrations are present.

ACPD
10, 3087–3127, 2010